Seismic System Reliability Analysis of Bridges using the Multiplicative Dimensional Reduction Method

Jin Zhang [a,b], Kaiming Bi [b], Shixiong Zheng [a], Hongyu Jia [a] and De-Yi Zhang [a,c*]

[a] *Department of Bridge Engineering, Southwest Jiaotong University, 610031 Chengdu, Sichuan, China*

[b] *Centre for Infrastructure Monitoring and Protection, School of Civil and Mechanical Engineering, Curtin University, Kent Street, Bentley WA 6102, Australia;*

[c] *Department of Engineering Mechanics, Ontario Power Generation, Ontario L1W 3J2 Canada*

ABSTRACT

A combined method of finite element reliability analysis and multiplicative dimensional reduction method (M-DRM) is proposed for systems reliability analysis of practical bridge structures. The probability distribution function of a structural response is derived based on the maximum entropy principle. To illustrate the accuracy and efficiency of the proposed approach, a simply-supported bridge structure is adopted and the failure probability obtained are compared with the Monte Carlo simulation method. The validated method is then applied for the system reliability analysis for a practical high-pier rigid frame railway bridge located at the seismic-prone region. The finite element model of the bridge is developed using OpenSees and the M-DRM method is used to analyse the structural system reliability under earthquake loading.

Key words: Multiplicative dimensional reduction method; Finite element reliability analysis; Principle of maximum entropy; Rigid frame bridge; System reliability analysis

1. INTRODUCTION

Reliable and efficient operation of large infrastructure systems such as road and highway networks is essential to life of people and prosperity of the entire society. These engineering systems usually consist of a number of sub-systems, -structures and -components that are likely to experience various failures during the service period, and engineering reliability analysis then become a useful tool for design, operation and maintenance of these engineering systems. Engineering structural reliability analysis normally bases on structural responses,

∗Correspondence to: De-Yi Zhang, Department of Engineering Mechanics, Ontario Power Generation, Ontario L1W 3J2 Canada
† E-mail: zhangdyhit@gmail.com.

which are normally evaluated by the finite element analysis (FEA) method considering the linear and/or nonlinear behaviour of structure elements (Zhang & Pandey, 2013; Wei & Rahman, 2010). Therefore, it is necessary to perform structural reliability analysis in conjunction with the FEA, which is often termed as finite element reliability analysis (FERA) (Balomenos & Pandey, 2016). However, it is commonly difficult for the engineers to have advanced programming experience and skills to connect FEA with reliability analysis techniques in the practical engineering design and analysis work.

Monte Carlo Simulation (MCS) (Rubinstein, 2008) can be used as a general and direct method for the FERA by repeatedly running the FEA code; however, it can become computationally expensive since the accuracy and efficiency depends on the total number of required simulations (Sudret & Kiureghian, 2002; Frangopol, 2008). The first-order and second-order reliability methods (FORM/SORM) are also the most commonly used approaches, which are based on the linear and quadratic approximations of the limit-state surface function, respectively. The FORM provides a direct scheme that can be used conveniently to get structural reliability index. The algorithms based on SORM require the computation of gradients and Hessians matrix of limit state function that cannot be easily obtained. Furthermore, both FORM and SORM cannot always provide results with desired accuracy, especially when the levels of uncertainty in the input parameters are high (Madsen, Krenk, & Lind, 1985; Rackwitz, 2001; Ditlevsen & Madsen, 1996).

Response surface method (RSM) is also commonly used in structural reliability analysis (Faravelli, 1989; Zheng & Das, 2000; Zhao, Liu, & Yang, 2016). The principle of RSM is to use a series of basis function to approximate the real complex performance function. Whether the response surface function and sampling points fit well or not is a key for the RSM. Furthermore, the criteria how to select samples and determine the sizes of those representative responses need further exploration (Zhang, Pandey, & Zhang, 2011).

Therefore, there is a need for an efficient method which can minimize the FEA computations and provide accurate approximation of the response probability distribution. Recently, the multiplicative dimensional reduction method (M-DRM) was proposed to approximate the FEA model by a surrogate function (Zhang & Pandey, 2013). Several examples are presented in Zhang and Pandey (2013) to illustrate the numerical accuracy and efficiency of the proposed method in comparison to the Monte Carlo simulation method. The M-DRM primarily includes, an additive decomposition of a multi-dimensional response function into multiple

one-dimensional functions, an approximation of response moments by moments of single random variable, and a moment-based quadrature rule for numerical integration. Thus the structural response moments can be calculated conveniently using M-DRM with a limited number of FEA evaluations. The probability distribution can then be estimated using the maximum entropy (MaxEnt) principle in combination with the fractional moments of the response. A small number of fractional moments with MaxEnt provide a highly accurate approximation of the response distribution.

From the perspective of application, Balomenos and Pandey (2016) used the M-DRM method for probabilistic analysis of two tested reinforced concrete slabs with and without shear reinforcement in the FEA platform ABAQUS. The results predicted by the deterministic FEA simulation show reasonable responses comparing to the behaviors of test specimens including the ultimate load, deflection and cracking pattern. The similar approach was used for nonlinear finite element analyses of reinforced concrete and steel frames based on OpenSees software (Balomenos & Pandey, 2016).

Following the above discussions, only few researches employed the M-DRM method for structural reliability analysis for single component or simple structures. In reality, the reliability assessment for complex structures is more worthy of attention. This paper has extended the application scope of M-DRM method into the actual complex engineering structures, the high-pier railway bridges, under earthquake loadings.

In recent years, many high-pier railway bridges have been constructed in Southwestern regions of China due to rapid economic development and the area's mountainous site topography (Wang & Gan, 2011). According to the statistics for Chinese high-pier railway bridges, around 90% of these bridges are located in the west of China, and approximately 40% of them have piers higher than 40m. Furthermore, these mountainous railway bridges with piers of varying heights usually have continuous and rigid frame girders in the superstructure and thin-walled hollow piers. Most of these bridges exceed the specification requirements and are different from highway bridges which have relatively flexible main girders (Cheng, Yang, Yeh & Chen, 2003). On the other hand, the southwest area of China, where these railway bridges are located, is a dense seismic zone (e.g., the 2008 Wenchuan Earthquake occurred on May 12, 2008 in Sichuan province with an earthquake magnitude of 8.0, and the Lushan Earthquake on April 20, 2013, also in Sichuan province, with an earthquake magnitude of 7.0) (Wang, 2008). Meanwhile, almost all the high-pier railway bridges built in the

mountainous area, such as the span lengths and pier heights, are beyond the range of seismic design codes (MRC, 2006).

Moreover, the seismic performance of high-pier railway bridges may be significantly different from that of highway or pedestrian bridges because of the special structural configurations and varying complex gully site conditions. For instance, the high-pier railway bridges in the substructure usually have high yet flexible piers, while the girders in the superstructure are often required to be more rigid in order to avoid derailment of high-speed trains and excessive vertical deflection caused by rail loads. Consequently, this has shed light on the importance and necessity of seismic analysis and the design of high-pier railway bridges in the southwestern regions of China (Caglayan, Ozakgul, Tezer & Uzgider, 2011; Liang, 2007). Therefore, it is of great importance to study the reliability of high-pier railway bridges under earthquake loading for real-world applications of seismic design and analysis.

This paper applies the M-DRM with MaxEnt approach for the complex structural system reliability analysis based on the structural responses evaluated from the FEA. A new multiplicative form of dimensional reduction method is adapted in this paper. First, the proposed reliability analysis method was applied for a simple supported highway bridge to validate its numerical accuracy and efficiency in comparison with the MCS, FORM and SORM. Then, based on the FEA software OpenSees, a high-pier rigid frame railway bridge was employed using the M-DRM scheme to analyze structural system reliability under earthquake loading.

2. THEORETICAL BACKGROUND AND NUMERICAL VALIDATION

2.1 Multiplicative dimensional reduction method

The N-dimensional integration for a continuous, differentiable, and real-valued function $\beta(\vec{\eta})$ having N variables $\vec{\eta}=\{\eta_1,\eta_2,\cdots,\eta_N\}\in R^N$ in the domain $\prod_{i=1}^{N}[a_i,b_i]$ can be defined as

$$I[\beta(\vec{\eta})]=\int_{a_N}^{b_N}\cdots\int_{a_1}^{b_1}\beta(\eta_1,\eta_2,\cdots,\eta_N)d\eta_1\cdots d\eta_N \tag{1}$$

By using the following linear transformation

$$\eta_i=\frac{b_i+a_i}{2}+\frac{b_i-a_i}{2}x_i, i=1,\cdots,N \tag{2}$$

The integration of Equation (1) can be transformed into the symmetric domain as

$$I[\varphi(\vec{x})]=\prod_{i=1}^{N}\frac{b_i-a_i}{2}\int_{-1}^{1}\cdots\int_{-1}^{1}\varphi(x_1,x_2,\cdots,x_N)dx_1\cdots dx_N \tag{3}$$

By using Taylor series expansion of $y=\varphi(\vec{x})$ at $\vec{x}=\vec{u}=\{u_1,\cdots,u_n\}^T$, Equation (3) can be expressed by (Rahman & Xu, 2004):

$$I[\varphi(\vec{x})]=I[y(\vec{u})]+\frac{1}{2!}\sum_{i=1}^{N}\frac{\partial^2 y}{\partial x_i^2}(\vec{u})I[x_i^2]+\frac{1}{4!}\sum_{i=1}^{N}\frac{\partial^4 y}{\partial x_i^4}(\vec{u})I[x_i^4]+\frac{1}{2!2!}\sum_{i<j}\frac{\partial^4 y}{\partial x_i^2\partial x_j^2}(\vec{u})I[x_i^2x_j^2]+\cdots, \tag{4}$$

where the terms $I[\prod_{i=1}^{N}x_i^{k_i}]$ vanish when k_i is an odd integer. Consider a univariate approximation:

$$\hat{\varphi}(\vec{x})=\hat{\varphi}(x_1,\cdots,x_N)=\sum_{i=1}^{N}\varphi(u,\cdots,u,x_i,u,\cdots,u)-(N-1)\varphi(u,\cdots,u) \tag{5}$$

where each term in the summation is a function of only one variable and can be subsequently expanded in a Taylor series at $\vec{x}=\vec{u}=\{u_1,\cdots,u_n\}^T$, and $\{u_1,\cdots,u_n\}^T$ represents the vector of random variables. The following Equation can then be derived

$$I[\hat{\varphi}(x)]=I[y(\vec{u})]+\frac{1}{2!}\sum_{i=1}^{N}\frac{\partial^2 y}{\partial x_i^2}(\vec{u})I[x_i^2]+\frac{1}{4!}\sum_{i=1}^{N}\frac{\partial^4 y}{\partial x_i^4}(\vec{u})I[x_i^4] \tag{6}$$

The univariate approximation leads to the residual error:

$$I[\varphi(\vec{x})]-I[\hat{\varphi}(\vec{x})]=\frac{1}{2!2!}\sum_{i<j}\frac{\partial^4 y}{\partial x_i^2\partial x_j^2}(\vec{u})I[x_i^2x_j^2]+\cdots \tag{7}$$

which includes the contributions from integrations of dimension two and higher. For sufficiently smooth $\varphi(\vec{x})$ with convergent Taylor series, the coefficients associated with higher-dimensional integrations are much smaller than that with one-dimensional integrations. In that case, terms associated with higher dimensional integrations can be neglected. In contrast, the residual error due to the second-order Taylor approximation $\tilde{\varphi}(\vec{x})$ can be given by

$$I[\varphi(\vec{x})]-I[\tilde{\varphi}(\vec{x})]=\frac{1}{4!}\sum_{i=1}^{N}\frac{\partial^4 y}{\partial x_i^4}(\vec{u})I[x_i^4]+\frac{1}{2!2!}\sum_{i<j}\frac{\partial^4 y}{\partial x_i^2\partial x_j^2}(\vec{u})I[x_i^2x_j^2]+\cdots \tag{8}$$

It should be noted that $I[\hat{\varphi}(x)]$ represents a reduced integration since only N number of one-dimensional integration is required, as opposed to one N-dimensional integration in $I[\varphi(x)]$. Furthermore, there is no need

to calculate the partial derivatives. If the contributions from two and higher dimensional integrations are negligibly small, $I[\hat{\varphi}(x)]$ provides a satisfactory approximation for $I[\varphi(x)]$.

As discussed in Introduction, in structural reliability analysis, the probability of failure for a specific failure mode is usually calculated through the numerical calculation of multiple integration for the limit state function. Due to the difficulty in achieving the multiple integration, the univariate dimensionality reduction method has been used in this paper to approximate the multiple integration by reducing the dimensionality of the integral and ensuring the adequate accuracy. The methodology of the used univariate dimensionality reduction method is presented through Equations (1) to (7), along with the approximation error estimated in Equation (7). In addition, the univariate dimensionality reduction method was compared with the second-order Taylor approximation scheme of Equation (8), and it is concluded that the approximation based on the univariate integration can achieve adequate accuracy for the multiple integral evaluation.

For a mechanical system with a random input vector of $\bar{X} = \{X_1, X_2, \cdots, X_n\} \in R^N$ that characterizes the uncertainty in loads, material properties, and geometry, $Y(\bar{X})$ represent a response of interest with the l^{th} statistical moment of

$$m_Y^l = \Theta[Y^l(\bar{X})] = \int_{R^N} y^l(\bar{x}) f_X(\bar{x}) d\bar{x} \tag{9}$$

where $f_X(\bar{x}) = f_{X_1}$ is the joint probability density function of $\bar{X}$ and Θ is the expectation operator. Following the dimension-reduction procedure, the l^{th} moment in Equation (9) can be approximated as

$$m_Y^l \cong \Theta[\hat{Y}^l(\bar{X})] = \Theta[\{\hat{\varphi}(\bar{x})\}] = \Theta[\{\sum_{i=1}^{N} \varphi(u_1, \cdots, u_{i-1}, x_i, u_{i+1}, \cdots, u_N) - (N-1)\varphi(u_1, \cdots, u_N)\}^l] \tag{10}$$

In traditional dimensional reduction method, Equation (10) Applying binomial formula:

$$m_Y^l \cong \Theta[\hat{Y}^l(\bar{X})] = \sum_{j=0}^{l} C_l^j \Theta\{[\sum_{i=1}^{N} \varphi(u_1, \cdots, u_{i-1}, x_i, u_{i+1}, \cdots, u_N)]^j \cdot [-(N-1)\varphi(u_1, \cdots, u_N)]^{l-j}\}, C_l^j = \frac{l!}{j!(l-j)!} \tag{11}$$

According to Zhang and Pandey (2013), it is proposed to apply the logarithmic transform of the response function, i.e., $\log[\varphi(\bar{x})]$, which drives a multiplicative form approximate model of the original function.

Consider a general response function, $y = \varphi(\bar{x})$, By using the logarithmic transformation, one can obtain:

$$\begin{gathered} \psi(\bar{x}) = \log(y) = \log[\varphi(\bar{x})] \\ \psi(u_1, \cdots, u_N) = \log[\varphi(u_1, \cdots, u_N)] \\ \psi(u_1, \cdots, u_{i-1}, x_i, u_{i+1}, \cdots, u_N) = \log[\varphi(u_1, \cdots, u_{i-1}, x_i, u_{i+1}, \cdots, u_N)] \end{gathered} \tag{12}$$

By using the inverse transformation, the original function can be written as

$$\begin{aligned}\exp[\psi(\vec{x})] &= \exp[\log(\varphi(\vec{x})] = \exp[\sum_{i=1}^{N}\psi(u_1,\cdots,u_{i-1},x_i,u_{i+1},\cdots,u_N)-(N-1)\eta(u_1,\cdots,u_N)] \\ &= \exp[(1-N)\psi(u_1,\cdots,u_N)\times\exp[\sum_{i=1}^{N}\psi(u_1,\cdots,u_{i-1},x_i,u_{i+1},\cdots,u_N)]\end{aligned} \tag{13}$$

Substitution of Equation (12) into Equation (13) leads to a multiplicative approximate of the response function in the following

$$\hat{\varphi}(\vec{x}) = \hat{\varphi}(x_1,\cdots,x_N) \approx [\varphi(u_1,\cdots,u_N)]^{1-N}\prod_{i=1}^{n}\varphi(u_1,\cdots,u_{i-1},x_i,u_{i+1},\cdots,u_N) \tag{14}$$

Then on obtains

$$\begin{aligned}m_Y^l \cong \Theta[\hat{Y}^l(\vec{X})] = \Theta[\{\hat{\varphi}(\vec{x})] &= \Theta[\{[\varphi(u_1,\cdots,u_N)]^{1-N}\prod_{i=1}^{n}\varphi(u_1,\cdots,u_{i-1},x_i,u_{i+1},\cdots,u_N)\}^l] \\ &= [\varphi(u_1,\cdots,u_N)]^{l-lN}\Theta\{\prod_{i=1}^{n}\varphi(u_1,\cdots,u_{i-1},x_i,u_{i+1},\cdots,u_N)\}^l\} \\ &= [\varphi(u_1,\cdots,u_N)]^{l-lN}\times\prod_{i=1}^{n}m_{\hat{Y}_i}^l\end{aligned} \tag{15}$$

The resultant moment evaluation in Equation (15) entails the *n*-fold numerical integration as *n* one-dimensional integrals, which is substantially more efficient. According to Equation (9), the *l*th-order moment of *Y* can be determined by the one-dimensional moment of

$$m_{\hat{Y}_i}^l = \Theta[Y^l(u_1,\cdots,u_{i-1},X_i,u_{i+1},\cdots,u_N)] = \int[Y(u_1,\cdots,u_{i-1},X_i,u_{i+1},\cdots,u_N)]^l f(X_i)dX_i \tag{16}$$

Using the Gaussian quadrature method, the one dimensional integral can be numerically approximated by a sum of weighted integrand items evaluated at the Gauss points (abscissas) as:

$$m_{\hat{Y}_i}^l = \Theta[Y^l(u_1,\cdots,u_{i-1},X_i,u_{i+1},\cdots,u_N)] = \int[Y(u_1,\cdots,u_{i-1},X_i,u_{i+1},\cdots,u_N)]^l f(X_i)dX_i \cong \sum_{k=1}^{N}w_i^k[Y(u_1,\cdots,u_{i-1},X_i^k,u_{i+1},\cdots,u_N)]^l \tag{17}$$

where w_i^k and X_i^k represent the *k*-th Gauss weight and abscissa (Gauss point), respectively; *N* is the quadrature order. For the normal and lognormal distribution, the Gaussian quadrature integration rule, including the quadrature weights and points, can be found from Zhang, Pandey, & Zhang (2011).

2.2 Probability distribution of structural response

After obtaining moments of structural response, the Maximum Entropy (MaxEnt) principle will be used for estimation of the probability distribution (Jaynes, 1957). The most unbiased probability distribution of a

random variable can be estimated by the MaxEnt principle by maximizing the entropy subjected to constraints from the available information such as moments of random variables.

The entropy of a continuous random variable having the probability density function (PDF) $f_Y(y)$ can be defined as

$$H[f] = -\int_Y f_y(y)\ln[f_Y(y)]dy \tag{20}$$

The PDF function $f_Y(y)$ can be derived based on the MaxEnt parameters (i.e., the Lagrange multipliers λ_i and the fractional exponents α_i). The MaxEnt parameters can be obtained following the optimization scheme proposed by Zhang & Pandey (2013) as

$$\begin{cases} find: \lambda_i \text{ and } \alpha_i \\ Minimize: D(\lambda,\alpha) = \ln[\int_Y \exp(-\sum_{i=0}^{l}\lambda_i y^{\alpha i})dy] + \sum_{i=1}^{m}\lambda_i m_Y^{\alpha_i} \end{cases} \tag{21}$$

A novel aspect of this computational approach is that the fractions α_i (i=1, 2,⋯,m) need not to be specified a priori as they are calculated via the above optimisation. Details behind the scheme of Equation (21) can be found in Zhang & Pandey (2013). This procedure has been implemented in the MATLAB using the simplex search method.

2.3 Numerical validation of linear structure under static loading

2.3.1 Problem description

A simply-supported concrete highway bridge shown in Figure 1 is used to illustrate and validate the accuracy and efficiency of the M-DRM method. C30 concrete is used for the bridge pier and deck. The bridge has a span length of 24m and the bridge deck width of 9.5m. The cross sections of bridge girder and pier are shown in Figure 1. All the loadings are applied according to the Chinese General Code for Design of Highway Bridges and Culverts (JTG D60-2004) (HPDI, 2004). The vertical deflection at middle span is required to be less than L/800=30mm in accordance with JTG D60-2004.

Eight random variables are considered with the distribution parameters in Table 1. Two variables related to the uncertainties of structural properties are considered, i.e. the Young's modulus of the concrete and moment of inertia of the beam cross-section. The other variables are all related to the loadings and the distribution of wind load is assumed to be lognormal while other loads follow the normal distribution.

Table 1.Statistical properties of random variables of the example bridge (linear)

Variable	Description	Distribution	Mean-value	Std.D	COV	Reference
E	Young's modulus	Normal	3.0E10 Pa	2.4E9 Pa	0.08	(Ellingwood & Rajashekhar, 1995)
Iz	Moment of inertia	Normal	0.828 m^4	0.041 m^4	0.05	Assumed
W1	Wind load	Lognormal	4.66KN	1.025KN	0.22	(Bartlett, Hong & Zhou, 2003)
W2	Wind load	Lognormal	5.46KN	1.201KN	0.22	
Q1	Lane load	Normal	21KN/m	4.41 KN/m	0.21	
Q2	Human load	Normal	4.5KN/m	0.945KN/m	0.21	
D	Gravity load	Normal	110KN/m	11.0KN/m	0.10	
P	Concentrated load	Normal	512KN	107.52 KN	0.21	

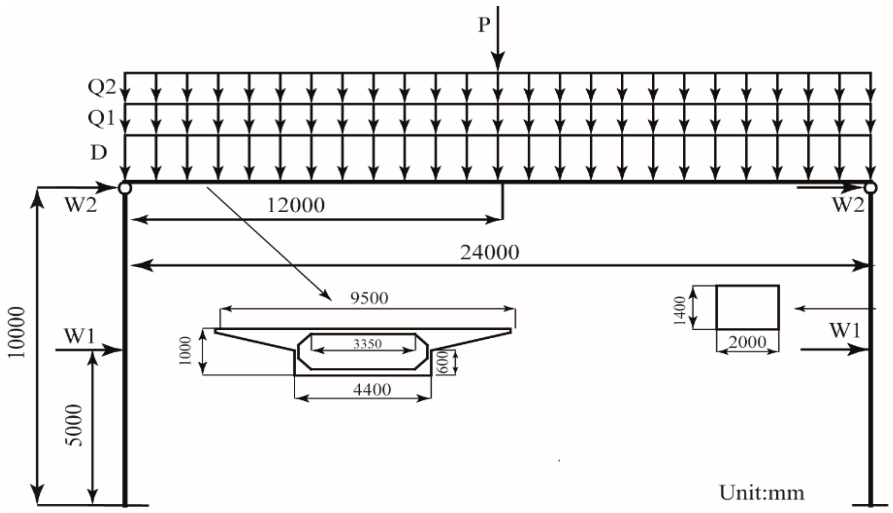

Figure1. Schematic view of a simply-supported railway bridge (linear) (unit: mm)

2.3.2 FERA analysis based on M-DRM

The FEA model of the simply-supported bridge is developed using the MATLAB software. The response is a product of 8 sub-functions due to the total of 8 random variables considered. Based on a fifth-order Gauss-Hermite integration scheme, a total of 41 structural analyses need to be performed to derive the distribution function of vertical deflection at the middle span. A schematic view of the input and output data in performing the FEA is given in Table 4.

To clearly elaborate on Table 4, a specific case with respect to the Young's modulus of concrete (E) is taken as an example. The five quadrature points are given in Table 2 and the rest random variables are fixed at their mean values. The vertical displacement at the middle span (Y) in each combination can be calculated using MATLAB and they are tabulated in the table as well. By following this manner, computations are repeated for all the other random variables. The mean and variance values of structural response can then be

calculated as $M_1 = \sum_{k=1}^{N} w_i Y$ and $M_2 = \sum_{k=1}^{N} w_i Y^2$ respectively. In fact, any fractional moment of order α_i can be approximated in a similar manner as $M_{\alpha_i} = \sum_{k=1}^{N} w_i Y^{\alpha_i}$. M_{ai} is the fractional moment, w_i represent Gauss weight and a_i represent the a_i-th order.

Table 2. Input and Output gird of structural response

Var.	N	X_J	E	…	P	Y(mm)	W_J	$W_J \times Y$	M1	$W_J \times Y^2$	M2
	1	-2.8570	2.96E+10	…	5.120E+05	22.8	0.011	0.257		5.853	
	2	-1.3556	2.98E+10	…	5.120E+05	22.7	0.222	5.041		114.436	
E	3	0	3.00E+10	…	5.120E+05	22.6	0.533	12.053	22.599	272.404	510.720
	4	1.3556	3.02E+10	…	5.120E+05	22.5	0.222	4.997		112.428	
	5	2.8570	3.04E+10	…	5.120E+05	22.3	0.111	0.251		5.599	
…	..	…	…	…	…	…	…	…	…	…	…
	36	-2.8570	3.00E+10	…	2.048E+05	19	0.011	0.214		4.065	
	37	-1.3556	3.00E+10	…	3.662E+05	20.9	0.222	4.641		97.007	
P	38	0	3.00E+10	…	5.120E+05	22.6	0.533	12.053	22.600	272.404	512.341
	39	1.3556	3.00E+10	…	6.578E+05	24.3	0.222	5.397		131.136	
	40	2.8570	3.00E+10	…	8.192E+05	26.2	0.111	0.295		7.729	
Mean	41		3.00E+10	…	5.120E+05	22.6					

As shown in Table 2, when the random variable E is considered, the other seven random variables are fixed at their mean values and the vertical displacement response Y at middle span can be conveniently obtained by calling the finite element analysis in MATLAB. The mean value M1 and second order raw moment M2 of displacement response Y can then be calculated. By following this manner, a total of 8 M1 and M2 will be calculated. In the last row of Table 4, the vertical displacement response is predicted using the mean values for all the random variables. Based on Equation (15), the integral statistics moment can be calculated using the simulation results for the single random variable. The results obtained from M-DRM are given in Table 3.

To demonstrate the accuracy of the proposed method, the results obtained from Metro Carlo simulation (MCS) method are also presented. Numerical results show that the mean, standard deviation and coefficient of variation obtained from these two methods are almost the same with a maximum relative error of 0.38%, which demonstrates the high accuracy of the proposed method. It should be noted that, to have the almost accurate results, only 41 trials are needed in the M-DRM method but 10^6 trials are required in the MCS method, meaning that the M-DRM method can significantly improve the efficiency of the calculation.

Table 3.Comparisons of the response statistics of the example highway bridge

	Vertical displacement at middle span (Y)		
Response statistics	M-DRM(41 Trials)	MCS(10^6 Trials)	Relative error (%)
Mean(mm)	22.6530	22.7348	0.38
Standard deviation	1.8462	1.8502	0.22
Coefficient of variation	0.0815	0.0814	0.16

Note: Relative error= |MDRM-MCS |/MCS

2.3.3 Failure probability of the highway bridge

After obtaining the statistic moments of structural responses in Section 3.2, the MaxEnt principle in Section 2.2 is applied to estimate the probability distribution of the vertical displacement response at middle span of the highway bridge. The MaxEnt optimisation can provide the Lagrange multipliers λ_i and fractional exponents α_i, which are listed in Table 4, and λ_i and α_i can then be used to derive the probability distribution function.

Table 4. MaxEnt distribution parameters for simply-supported bridge(linear)

Fractional moments	Entropy	k	0	1	2	3
m=3	2.28	λ_i	31.4231	-1.1464	0.5891	0.0277
		α_i		1.8155	1.9980	1.0078

Figure 2 compares the PDFs of the middle span vertical displacement using the MCS and M-DRM methods, which shows that the PDF results resulting from two methods agree with each other very well.

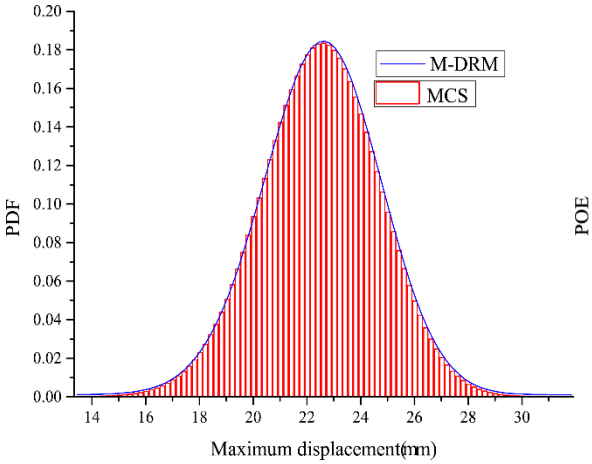

Figure 2. PDF of the vertical displacement

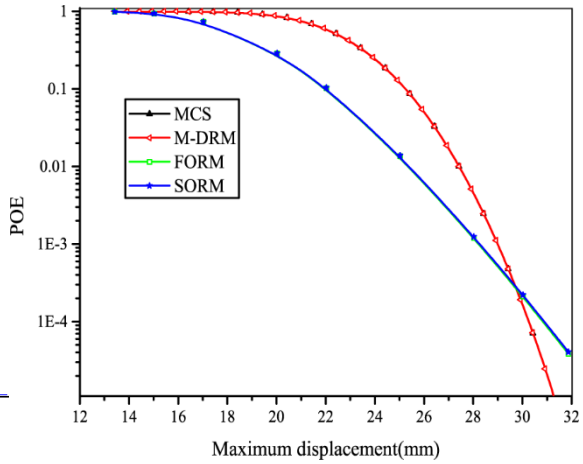

Figure 3. POE of the vertical displacement

In order to further illustrate the accuracy of M-DRM, Figure 3 presents the probability of exceedance (POE) of the vertical displacement at middle span using MCS, M-DRM, FORM and SORM methods. It is

seen that the POE curve for vertical displacement at middle span using the M-DRM is consistent with that of MCS, while the results from FORM and SORM have large difference with that of MCS. Specifically, Table 5 gives the results of failure probability calculated by MCS method using a total of 10^6 samples and the other three methods M-DRM, FORM and SORM. It is observed that M-DRM method lead to accurate estimation of failure probability with only a relative error of 5.8%, while the relative errors for the FORM and SORM methods are 42.6% and 36.1%, respectively.

Table 5. Failure probability obtained by different methods

Method	MCS	M-DRM	FORM	SORM
Failure probability	1.55×10^{-4}	1.64×10^{-4}	2.21×10^{-4}	2.11×10^{-4}
Error (%)	-	5.8	42.3	36.1

2.4 Numerical validation of nonlinear structure under dynamic loading

2.4.1 Problem description

The same simply-supported concrete highway bridge of Figure 4 is used to validate the accuracy and efficiency of the M-DRM method by using the nonlinear structure under dynamic loading. The parameters of the structure are described in Section 2.3.1 in addition to the nonlinear material models and input ground motion provided in this section.

The cross section of the pier is shown in Figure 4 and a total of 44 longitudinal reinforcement bars (a diameter of 22mm) are used having the longitudinal reinforcement ratio of 0.59%. The stirrup rebar has a diameter of 12mm, the spacing of 100 mm and the volumetric reinforcement ratios of 0.64%. The bottom of the two piers are fixed and the pile-soil-interaction is not considered.

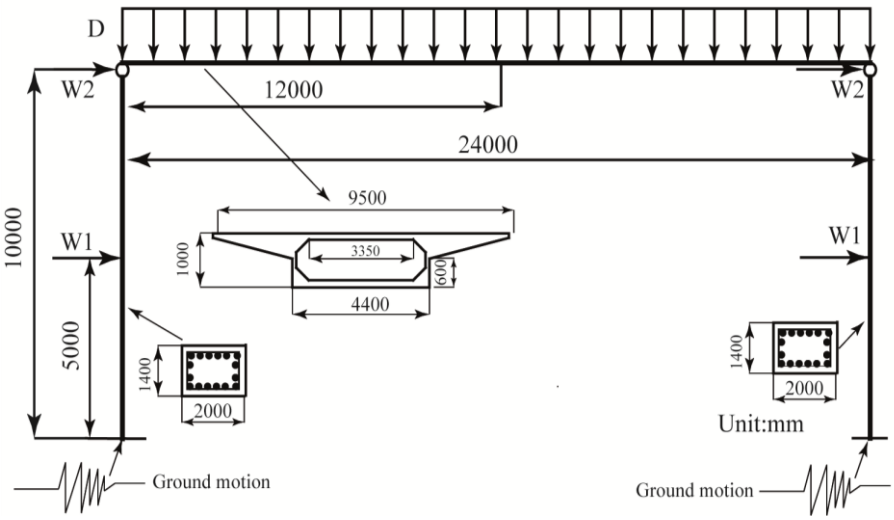

Figure 4. Schematic view of a simply-supported railway bridge (nonlinear analysis) (unit: mm)

2.4.1.1 Ground motions

The 1979 Imperial Valley earthquake (magnitude 6.53) motions are used. The ground motion has a PGA of 0.162g and a PGD of 0.042m and are shown in the following Figure 5.

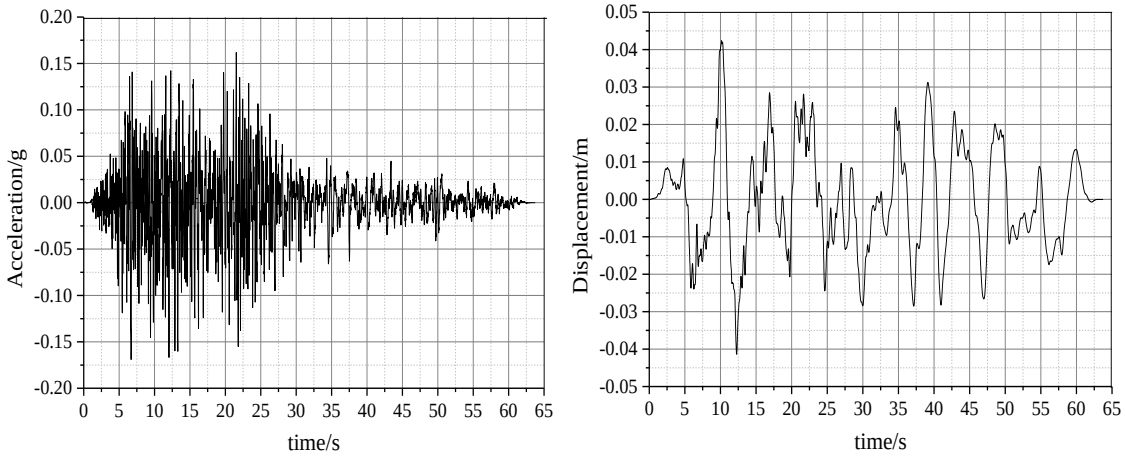

(a) Acceleration (b) Displacement

Figure 5. Ground motion record for the 1979 Imperial Valley earthquake.

2.4.1.2 Uncertainties of bridge structure

A total of nine random variables are considered in the present study and are listed in Table 6. These variables can be categorized into three groups, i.e. the parameters for the pier, girder and load. The variables associated with piers are the Young's modulus and strength of concrete and steel. The variables for the bridge girder are the Young's modulus and compressive strength of concrete. The distribution of the wind load is assumed to be the lognormal and the gravity loading follows the normal distribution. The mean, standard deviations and coefficient of variations for all the variables are listed in Table 6.

Table 6. Statistical properties of random variables for the bridge (nonlinear analysis)

Component	Variable	Description	Distribution	Mean	Std.D	COV	Reference
Piers	Ec1	Young's modulus of concrete	Normal	3.00E10 Pa	2.40E9Pa	0.080	(Ellingwood & Rajashekhar, 1995)
	Fc1	compressive strength of concrete	Normal	2.01E7 Pa	2.71E6Pa	0.135	(Nowak, Rakoczy, & Szeliga, 2011)
	Es	Young's modulus of steel	Normal	2.00E10 Pa	6.60E8Pa	0.033	(Mirza & Skrabek1991)
	Fy	yield strength of steel	Normal	3.35E8 Pa	1.34E7Pa	0.040	(A. Nowak, S. Nowak & Szerszen, 2003)
Girder	Ec2	Young's modulus of concrete	Normal	3.00E10 Pa	2.40E9Pa	0.080	(Ellingwood & Rajashekhar, 1995)
	Fc2	compressive strength of concrete	Normal	2.01E7 Pa	2.71E6Pa	0.135	(Nowak, Rakoczy, & Szeliga, 2011)
Load	W1	Wind load	Lognormal	4.66KN	1.025KN	0.22	(Bartlett, Hong & Zhou, 2003)

W2	Wind load	Lognormal	5.46KN	1.201KN	0.22
D	Gravity load	Normal	110KN/m	11.0KN/m	0.10

2.4.2 FERA analysis based on M-DRM

The FEA model of the simply-supported bridge with nonlinear material is developed using the OpenSees software. Due to the 9 random variables considered, a total of 46 structural analyses need to be performed to derive the distribution function for the curvature response at bottom section of the pier based on a fifth-order Gauss-Hermite integration scheme.

2.4.2.1 Finite element modelling

To assess the nonlinear behaviours of the simple supported bridge under earthquake loading, the finite element model is developed in the OpenSees software. Since there is very less severe damage of the bridge girder observed during an earthquake, it is assumed that the girder remains linear elastic in the present study and is modelled using the elastic beam column element. For the bridge piers, they may experience significant nonlinear deformation during a severe earthquake due to the height, and thus are modelled by the nonlinear beam column element.

The uniaxial material Concrete02 is used to model the concrete in the deck and piers. Material Steel01 is used to model the reinforcement bar in the piers. The constitutive models for different material models are presented in Figure 5. For the constitutive model of steel01 in Figure 6(a), σ_y is the yield strength of steel bar with a value of 335MPa, E represents the initial elastic tangent having a value of 200GPa, and b is ratio between post-yield tangent and initial elastic tangent with a value of 0.01.

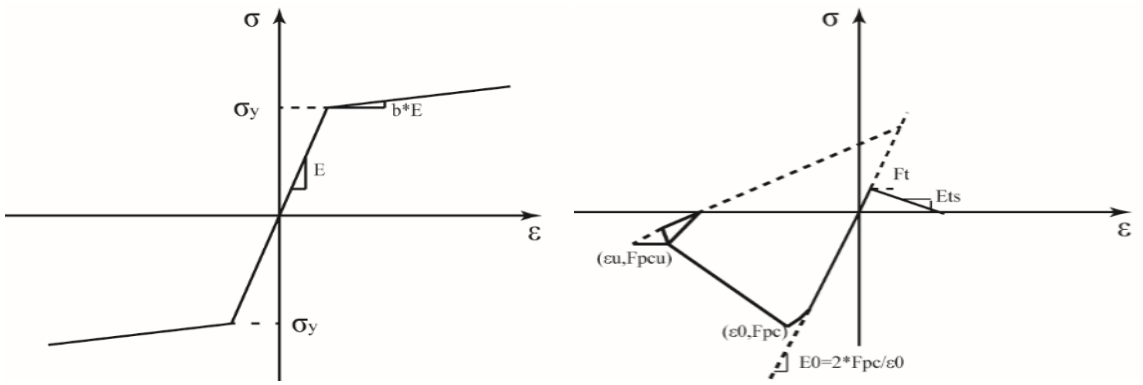

a) Steel01 b) Concrete02

Figure 6. Nonlinear material models

Figure 6(b) shows the constitutive model of Concrete02, where F_{pc} is the 28-day concrete compressive strength equalling 20.1MPa, F_{pcu} is concrete ultimate compressive strength with the value of 4.68MPa, E_{ts} is the tension softening stiffness with a value of 100, F_t is the concrete tensile strength with the value of 3.28MPa, ε_0 is the concrete strain at maximum strength equalling 0.002, and ε_u is concrete ultimate strain having a value of 0.004.

2.4.2.1 Failure probability of the bridge under earthquake loading

A total of 46 transient analyses are carried out in the OpenSees using the Imperial Valley ground motion of Figure 5. Figures 7 (a) and (b) present the mean displacement time history responses at the top of pier and the mean curvature response of the bottom section of pier. The maximum displacement response at the top of pier is 0.009m at 20.02s, and the maximum curvature of the bottom section of pier is 7.35e-4 at 20.02s.

After the structural response of interest has been obtained, the MaxEnt principle is used to estimate the probability distribution for the bearing and the system. The Lagrange multipliers λ_i and fractional exponents α_i are derived based on the MaxEnt optimization scheme for the bridge response and are presented in Table 7.

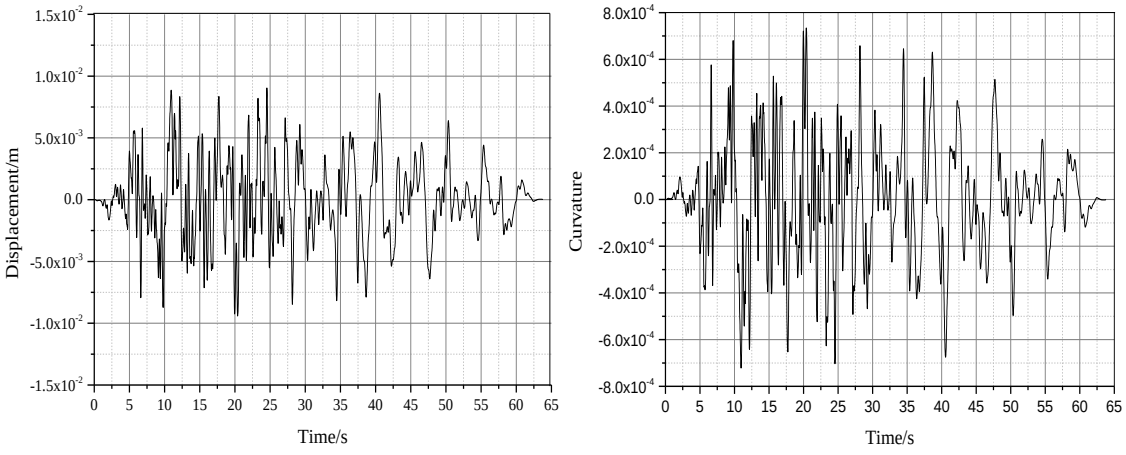

a) Displacement history at top of pier b) Curvature history of the bottom section of pier

Figure 7. Dynamic response of bridge under the Imperial Valley ground motion

Table7. MaxEnt distribution parameters for simply-supported bridge (nonlinear analysis)

	Entropy	k	0	1	2	3
Bearing	7.53e-8	λ_i	-43.1994	-6.6819	0.9119	58.5415
		α_i		1.7644	2.5219	0.3987

The PDF of the maximum curvature at the bottom section of the pier is shown in Figure 8. The PDF curve of the maximum curvature using the M-DRM method agree well with the one by the MCS method. To further illustrate the accuracy of the M-DRM method, Figure 9 presents the probability of exceedance (POE) of the maximum curvature at the bottom section of the pier using both MCS and M-DRM methods. It is seen from Figure 9 that the POE curve derived by the M-DRM method is consistent with the one by the MCS method with a maximum relative error of 1%.

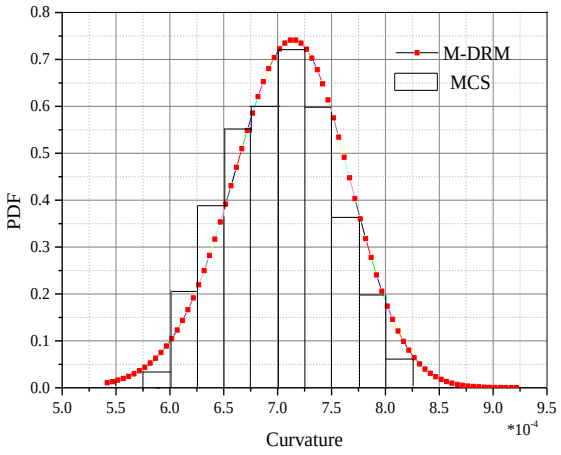

Figure 8. PDF of the curvature at the bottom section of the pier

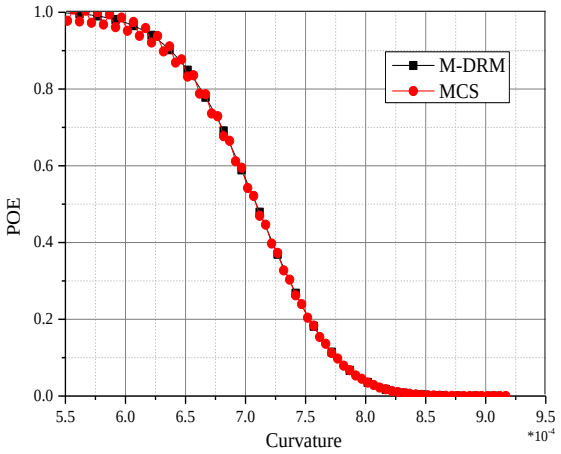

Figure 9. POE of the curvature at the bottom section of the pier

3. PRACTICAL APPLICATION: RELIABILITY ASSESSMENT OF A HIGH-PIER RAILWAY BRIDGE

3.1 Description of the bridge

A large-span high-pier continuous rigid frame highway bridge located in Guizhou province, China is employed to be studied. Figure 4 shows the schematic view of the bridge. The prestressed-concrete continuous rigid frame bridge is located at a V-shaped canyon site. The span lengths of the bridge are 89, 168 and 89 m, respectively. The cross sections of the bridge deck along the longitudinal direction vary with the locations, with the maximum height appearing at the pier. Two typical cross-sections of the bridge girder are presented in Figure 10.

Because of the site conditions, two high piers were designed for the bridge. The pier heights reach 75m and 103 m, respectively, at Piers #1 and #2. The dimensions of the pier also vary with the pier height. Three typical cross sections of the pier are given in Figure 4. In the 3-3, 4-4 and 5-5 section views, a total of 584, 768 and 801 longitudinal reinforcement bars with a diameter of 22 mm are used, with the longitudinal reinforcement ratio of 0.44%, 0.24% and 0.18%, respectively. The diameter of the stirrup is 12 mm. The distance between adjacent stirrups is 100 mm. For Piers #1 and #2, the volumetric reinforcement ratios for the stirrup are 0.56% and 0.63%, respectively. Since the main girder is not a vulnerable component of this type of bridge, only the concrete without accounting for reinforced bars are considered in the modelling. All the degrees of freedom at the bottom of the two piers are fixed and the pile-soil interaction are not considered.

3.2 Finite element modelling

To assess the nonlinear behaviours of the rigid frame bridge under earthquake loading, the 3D finite element model is developed in the OpenSees software. Since there is normally very less severe damage of the bridge deck observed for the rigid frame bridge during an earthquake, it is assumed that the deck remain linear elastic in the present study and is modelled using the elastic beam column element. For the bridge piers, they may experience significant nonlinear deformation during a severe earthquake due to the height, and thus are modelled by the nonlinear beam column element. The modelling scheme for bridge deck and piers are similar to that used in Ref. (Matthew & Greg 2008). Bearings may also experience damage under earthquake loading,

and they are modelled by the two node link element in OpenSees (i.e., TwoNodeLink) (Mazzoni, McKenna, Scott, & Fenves, 2006). TwoNodeLink element is defined by two nodes and can have a zero or non-zero length. This element can also have 1 to 6 degrees of freedom, where only the transverse and rotational degrees of freedom are coupled as long as the element has non-zero length.

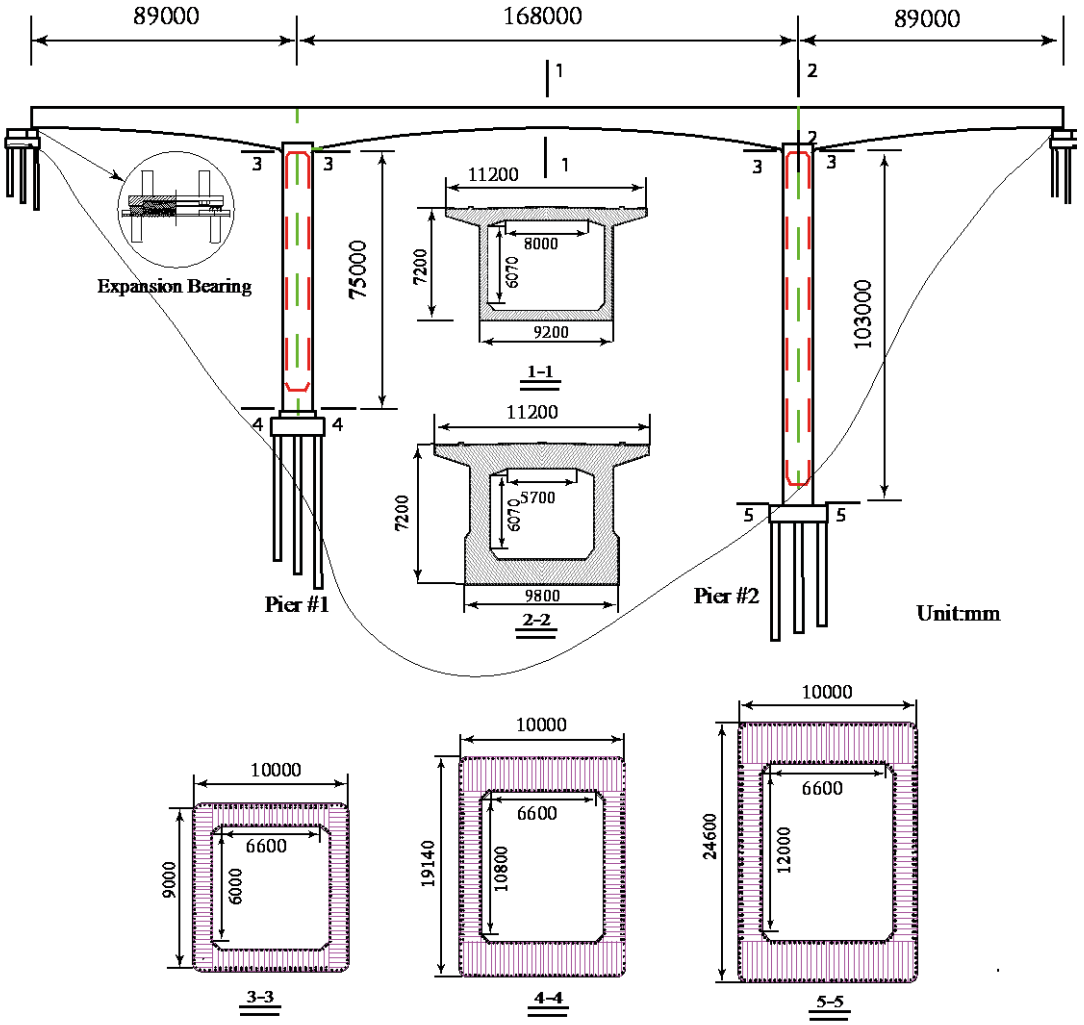

Figure 10. Schematic view of the high-pier railway bridge

The uniaxial material Concrete02 is used to model the concrete in the deck and piers. Material Steel01 is used to model the reinforcement bar in the piers. For the bearings at the expansion joint, the hardening uniaxial-material is adopted to model the longitudinal nonlinear behaviour of the bearings. The constitutive models for different material models are presented in Figure 11. For the constitutive model of steel01 in Figure11(a), σ_y is the yield strength of steel bar with a value of 335 MPa in, E represents the initial elastic tangent having a value of 210GPa, and b is ratio between post-yield tangent and initial elastic tangent with a value of 0.01.

Figure 11(b) shows the constitutive model of Concrete02, where F_{pc} is the concrete compressive strength at 28 days equalling to 23.4MPa, F_{pcu} is concrete compressive strength at ultimate state with a value of 4.68MPa, E_{ts} is the tension softening stiffness with a value of 100, F_t is the concrete tensile strength with the value of 3.28Mpa, ε_0 is the concrete strain at maximum strength equalling 0.002, and ε_u is concrete ultimate strain have a value of 0.004.

In the constitutive model of Hardening, as shown in 11(c), F_y is the yield force of bearing, according to the bearing reaction force analysis, the value can be used 192.52KN. X is yield deformation, according to the actual bearing and literature (MRC, 2013), the value is 0.004. b is ratio between post-yield tangent and initial elastic tangent, equal to 0.0001.

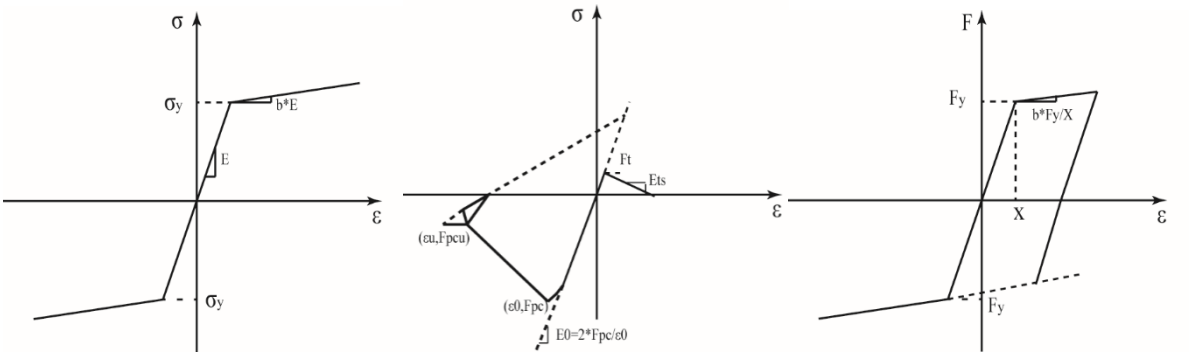

a) Steel01 b) Concrete02 c) Hardening

Figure 11. Material models

3.3 Uncertainty of inputs

3.3.1 Uncertainties of bridge structure

.A total of eight random variables are considered in the present study and they are listed in Table 8. These variables can be divided into four different categories, i.e. the parameters related to the pier, girder, bearing and system. The variables associated with piers are the Young's modulus and strength of concrete and steel; the corresponding variables related to the bridge girder are the Young's modulus and compressive strength of the concrete. The possible variations on the bearing friction factor and damping ratio of system are also considered in the present study. Lognormal distribution is assumed for the friction factor of the bearing, all other parameters are assumed following a normal distribution. The mean values, standard deviations and coefficient of variations of all the variables are tabulated in Table 8.

Table 8. Statistical properties of random variables of the rigid frame bridge

component	Variable	Description	Distribution	Mean	Std.D	COV	Reference
Piers	Ec1	Young's modulus of concrete	Normal	3.25E10 Pa	2.60E9Pa	0.080	(Ellingwood & Rajashekhar, 1995)
	Fc1	compressive strength of concrete	Normal	2.86E7 Pa	3.86E6Pa	0.135	(Nowak, Rakoczy, & Szeliga, 2011)
	Es	Young's modulus of steel	Normal	2.00E10 Pa	6.60E8Pa	0.033	(Mirza & Skrabek1991)
	Fy	yield strength of steel	Normal	3.35E8 Pa	1.34E7Pa	0.040	(A. Nowak, S. Nowak & Szerszen, 2003)
Girder	Ec2	Young's modulus of concrete	Normal	3.55E10 Pa	2.84E9Pa	0.080	(Ellingwood & Rajashekhar, 1995)
	Fc2	compressive strength of concrete	Normal	3.93E7 Pa	5.31E6Pa	0.135	(Nowak, Rakoczy, & Szeliga, 2011))
Bearing	u	Friction factor	Lognormal	0.02	0.002	0.100	Assumed
System	ξ	Damping ratio	Normal	0.05	0.005	0.100	(Nielson & Desroches, 2007).

3.3.2 Uncertainty of ground motions

Selection of input ground motions for seismic analysis, especially for the nonlinear dynamic analysis of structures, is changeling. This is because that a slight fluctuations in the inputs can lead to significant differences in the output structural responses. In the engineering practice, either the recorded or the synthesized ground motions are normally used. In the present study, the synthesized ground motions are used due to a lack of ground motion records in Guizhou Province, China.

The spectral representation method proposed by Bi and Hao (2012) is used to generate the ground motion time histories. A total 30 ground motions are generated to be compatible with the design acceleration response spectrum from the Fundamental Code for Design on Railway Bridge and Culvert (J460-2005) (MRC, 2005).

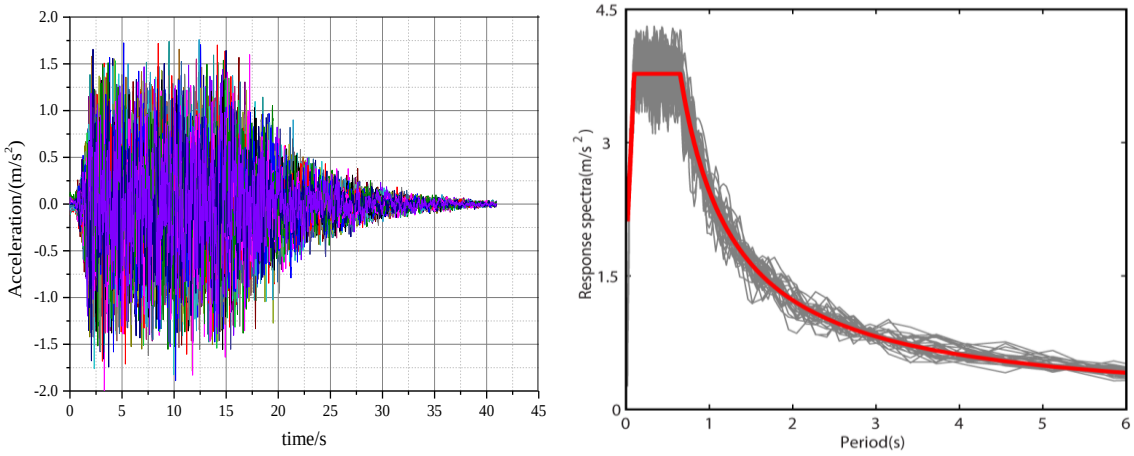

a) 30 synthetic ground motions b) Simulated and target response spectra

Figure 12. Simulated ground motions and response spectra

According to the site-specific probabilistic seismic hazard analysis for the Chahe Railway bridge (GSB, 2010), the seismic intensity of the high-pier railway bridge is moment magnitude Mw=7 with the design PGA of 0.15g and the site predominant period of 0.65s. The time duration of the synthesis ground motions is 40.96 s. Figure 12(a) shows the simulated acceleration time histories and good compatibility are observed in Figure 12(b). Based on the ground motion selection requirements and recommendations under JTG/T B02-01 (MTC, 2008) and FEMA P-695 (ATC, 2008), the total 30 synthetic ground motions can well represent the design response spectra of the bridge.

3.4 Failure modes of RFB

The primary failure modes for the high-pier railway bridge include the failure of bearing displacement exceeding the limit and the pier ductility failure.

3.4.1 Bearing failure

The limit state function of bearing failure can be expressed as (MRC, 2013):

$$D_{LS} \geq D_{LSO} \tag{22}$$

where D_{LS} is the peak value of displacement response of bearing under earthquake loading, and D_{LSO} is the limit displacement of bearing. In the present study for the pot type expansion bearing, D_{LSO} is defined as 0.30m in according with the specification in Ref. (MRC, 2013).

3.4.2 Failure of pier

Damage to a column can be determined using the relative displacement ductility ratio of the column, namely (Hwang, Liu, & Chiu, 2001),

$$\mu_d = \frac{\Delta}{\Delta_{cy1}} \tag{23}$$

where Δ is the relative displacement of a column obtained from seismic response analysis of the bridge, and Δ_{cy1} is the relative displacement of a column when the vertical reinforcing bars begin to yield. In Hwang's study (Hwang, Liu, & Chiu, 2001) , according to the displacement ductility ratios, column damages can be categorized into four states, including the slight damage, moderate damage, extensive damage and complete

damage, with the respective ductility ratios of $\mu_{cy1}=1.0$, $\mu_{cy}=1.2$, $\mu_{c2}=1.76$, and $\mu_{cmax}=4.76$. In this study, the complete damage state of the piers are defined as the ultimate limit state, i.e., the ductility ratio of $\mu_d=4.76$ is selected.

At the first yielding, the relative displacement at top of the column can be calculated as (MTC, 2008):

$$\Delta_{cy1}=\frac{2\phi_1(L/2)^2}{3} \tag{24}$$

in which, ϕ_1 is the cross-section curvature when the vertical reinforcing bars reach the first yield, L the column height with $L_1=75\,m$ and $L_2=103\,m$, respectively, for Pier #1 and Pier #2.The relationship of bending moment and curvature at different sections of Piers #1 and #2 are shown in Figure 13 based on a pushover analysis in OpenSees.

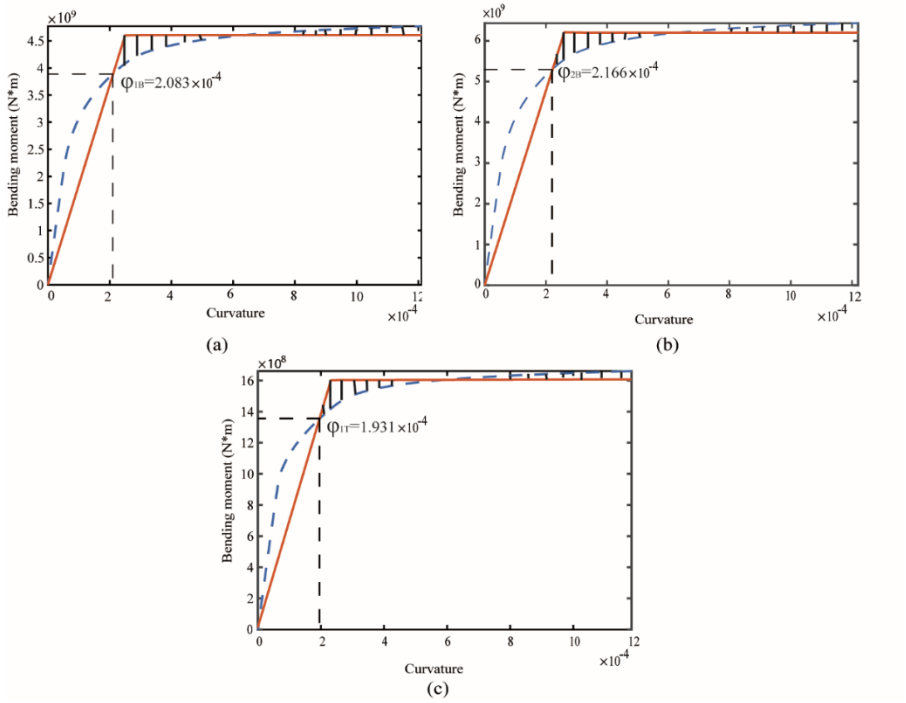

Figure 13. Relationship between bending moment and curvature: (a) bottom of pier #1 (b) bottom of pier #2 (c) top of piers #1 and #2

In Figure13, the blue curves represent actual relationships of the bending moment and curvature of three sections. It can be easily found, as the curvatures of the sections increase, the bending moments of the sections increase gradually, and then tend to be stable, the maximum bending moments of 3-3, 4-4 and 5-5 section are

446 $4.75\times10^{9}\ N\cdot m$, $6.45\times10^{9}\ N\cdot m$ and $1.62\times10^{9}\ N\cdot m$, respectively. The red curves are the equal relationships of
447 bending moment and curvature of three sections, which are gotten by the proposed method in the Guidelines
448 for seismic design of bridge (MTC, 2008). For example in Figure 13(a), we can switch the blue curve to red
449 curve in accordance with two shaded areas are equal. When the red curve and blue curve are drown together,
450 the first intersection of two curves is the point that vertical reinforcing bars reach begin to yield in the section.
451 Like this, we can conveniently get the yield curvature of three cross sections, then according Equation (24)
452 and (23), the relative displacement ductility ratio are calculated.

453 *3.4.3 Structural system failure*

454 After determining the failures for the bridge bearings and piers, the limit state equations of the structural system
455 can be calculated. The generalized multidimensional threshold limit state (MTLS) function provides a tool that
456 allows considering these dependencies among different components of the threshold vector related to different
457 quantities. The MTLS function L(R, R_{lim}) are used for the case when *n* different types of response parameters
458 considered simultaneously, and can be defined in a *n*-dimensional form (a mathematical "surface") as
459 (Cimellaro, Reinhorn, Bruneau, & Rutenberg, 2006):

460 $$L(R_1,\cdots,R_n)=\sum_{i=1}^{n}\left(\frac{R_i}{R_{i\lim}}\right)^{Ni}-1 \tag{25}$$

461 where $R_i = ith$ component of the response vector (e.g., drifts, accelerations, forces, velocities, etc.); $R_{i\lim} = ith$
462 component of the threshold vector, representing the one-dimensional limit states; and Ni= interaction factors
463 determining the shape of the n-dimensional surface.

464 In the above proposed formulation, the limit states can be considered either linear or nonlinear dependent
465 and independent. All these options can be formulated as the particular cases from the more general one with
466 suitable parameters. For the bi-dimensional case in this study, the proposed multidimensional threshold limit
467 state can be expressed by

468 $$\left(\frac{\varphi_{LS}}{\varphi_{LSO}}\right)^{N_\varphi}+\left(\frac{D_{LS}}{D_{LSO}}\right)^{N_D}-1=0 \tag{26}$$

where φ_{LSO} and D_{LSO} = pier displacement ductility ratio and bearing displacement thresholds, their values are 4.76 and 0.30, respectively; φ_{LS} and D_{LS} = displacement response ductility ratio of pier and peak displacement response of bearing, respectively; N_{φ} and N_D =coefficients determining the shape of the limit state surface.

A simpler expression is obtained by assuming $N_{\varphi}=1$ and according to (Cimellaro, Reinhorn, Bruneau, & Rutenberg, 2006), $N_D=2$, which results in:

$$(\frac{\varphi_{LS}}{\varphi_{LSO}})+(\frac{D_{LS}}{D_{LSO}})^2-1=0 \tag{27}$$

which is the final limit state function of system. Based on Equation (27), on can conveniently combine the limit state equations for each single component into the limit state equation of the structural system. Then the limit state equation of the structural system can be used as the objective function to analyze the structural system reliability using the M-DRM method.

3.5 Failure probability of RFB

After the limit state functions of the components (bearings and piers) and structural system are developed, the transient analysis can be performed in the OpenSees to obtain the structural responses under the simulated 30 ground motions given in Figure 12. Because a total of 8 random variables are considered and each variable corresponds to five Gaussian interpolation points, the finite element calculation needs to be performed 41 times under each ground motion (including the calculation for mean values of each variable). Therefore, a total of 1230 transient analyses are carried out in the OpenSees. Figures 14 (a) and (b) present the typical displacement time history responses of bearings and piers under the #1 ground motion.

As shown in Figures 14(a) and (b), the displacement responses of bearing show the consistent variation trend with that of pier for both #1 bearing and pier and #2 bearing and pier. This is due to the fact that well-integral deformation can be maintained for the rigid frame bridge. Specifically, the peak displacement of #1 bearing is slightly larger than that of #1 pier due to the axial deformation of the bridge deck. Under #1 ground motion, the peak displacement of #1 bearing is 0.1082m while that for #1 pier is 0.0785m.

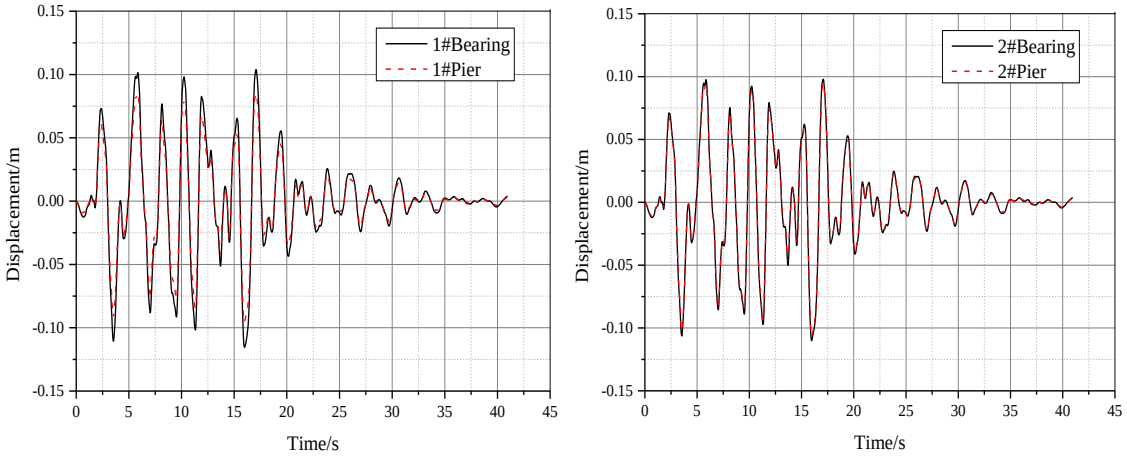

(a) #1 bearing and pier (b) #2 bearing and pier

Figure 14. Displacement response under #1 ground motion

It should be noted that peak value of structural response in the limit state functions is used. According to Li et al. (Li, Chen, & Fan, 2007), an equivalent extreme-value function can be used for the multiple components that have same failure mode. For the bearings:

$$D_{LS} = Minimum(D_{LS1}, D_{LS2}) \tag{28}$$

D_{LS1}, D_{LS2} are the peak longitudinal displacement response of #1 bearing and #2 bearing, respectively. For example, under #1 ground motion, the values of D_{LS1} and D_{LS2} are 0.1082m, 0.0995m, respectively, resulting in a value of 0.1082m for D_{LS}.

For the bridge piers, according to Equations (23) and (24), the relative displacements of piers #1 and #2 can be obtained when the plastic hinges are formed. Also equivalent extreme-value function can be expressed as:

$$\Delta_{cy} = Minimum(\Delta_{cy1T}, \Delta_{cy1B}, \Delta_{cy2B}) \tag{29}$$

in which $\Delta_{cy1T}, \Delta_{cy1B}$ and Δ_{cy2B} are the relative displacements of pier when the plastic hinges are formed at Sections 3-3, 4-4 and 5-5, respectively. According to Equation (24), the values of $\Delta_{cy1T}, \Delta_{cy1B}$ and Δ_{cy2B} are 0.1810m, 0.1953m and 0.3830m, respectively, in this study, so the value of Δ_{cy} is 0.1810m. It is found that the top section of #1 pier will form the plastic hinge firstly.

As discussed in Section 4.4.2, the serious damage state is considered as the limit state in the reliability analysis for piers, with the relative displacement ductility ratio μ_d of 4.76. According to Equation (30), when the serious damage occur first at #1 pier, the relative displacement Δ of #1 pier is 0.8616m. Comparing with the failure displacement of bearing $D_{LSO} = 0.25m$, the failure displacement of #1 pier is larger. This means that the bearing failure will occur prior to the failure of piers under rare earthquake loading.

After the structural response of interest was obtained, the MaxEnt principle is used to estimate the probability distribution of bearing and system. Then, λ_i and α_i are used to define the probability distribution function. The MaxEnt optimization gives the Lagrange multipliers λ_i and the fractional exponents α_i for the bridge response under #1 ground motion in Table 9.

Table 9. MaxEnt distribution parameters of the bridge under #1 ground motion

	Entropy	k	0	1	2	3
Bearing	9.65e-9	λ_i	-232.4229	335.2931	82.6674	145.1932
		α_i		-0.9526	-36.2530	0.1347
	Entropy	k	0	1	2	3
System	4.07e-10	λ_i	-92.4705	26.7038	22.1701	110.9979
		α_i		0.4838	-0.2410	-1.0642

The probability distribution of displacement response of #1 bearing under #1 ground motion is shown in Figure 15(a). It can be seen that, under the #1 ground motion excitation, the probability density value of the displacement response of #1 bearing is 0.161 at the displacement of 0.132m, which is also the maximum possible displacement response. For the structural system, the maximum probability density value is 0.527 at the system ratio of 0.667, as shown in Figure 15(b).

Finally, the failure probability of bearing and system of rigid frame bridge under 30 ground motions is listed in Table 10 and shown in Figure 16. It is seen from Figure16 that the maximum failure probability of the bearing is $2.722*10^{-4}$ under #13 ground motion. In contrast, the failure probability of the structural system is greater than that of the bearing, meaning that it is not safe to simply use the failure probability of the structural system with the failure probability of a component. Similarly, the maximum failure probability of structural system is $6.265*10^{-4}$under #13 ground motion. The failure probability varies with ground motions obviously for either the structural bearing or system and uncertainty of the ground motions affects the structural

failure probability much more than the structural parameters. The average failure probabilities of bearing and structural systems under the total 30 ground motions are $1.071*10^{-4}$ and $2.466*10^{-4}$, respectively.

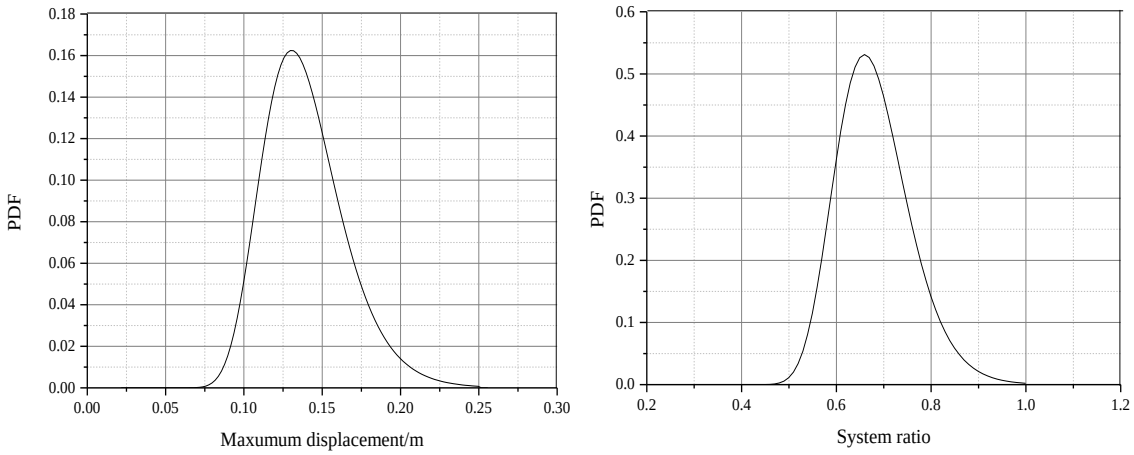

a) #1 Bearing b) System

Figure 15. PDF of the #1 bearing and structural system

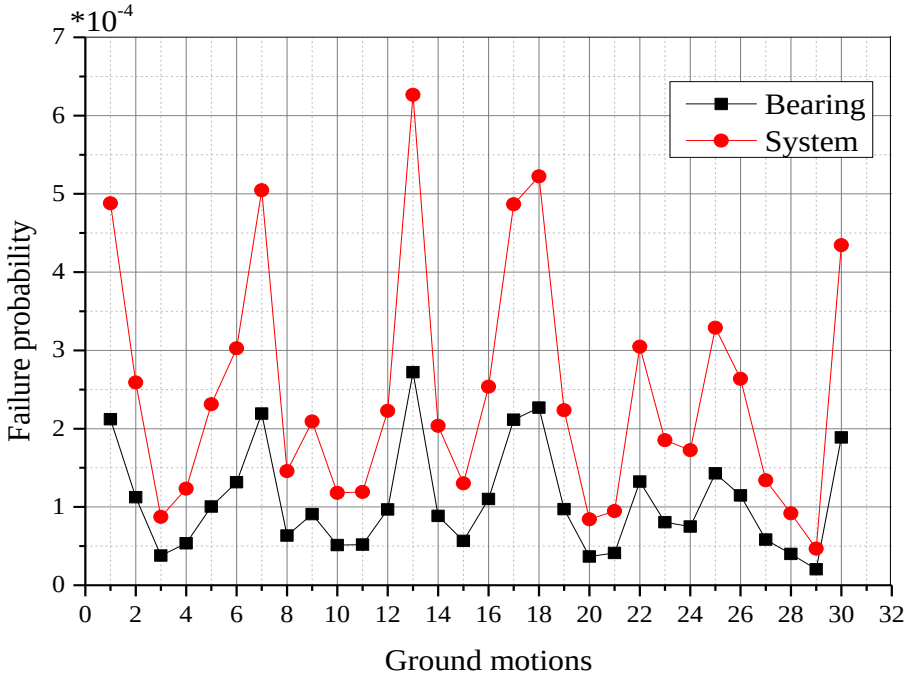

Figure16. Failure probability of the high-pier railway bridge under earthquake loading

Table10. Failure probability of the high-pier railway bridge under 30 ground motions ($*10^{-4}$)

Ground motion	No.1	No.2	No.3	No.4	No.5	No.6	No.7	No.8	No.9	No.10
Bearing	2.120	1.125	0.379	0.536	1.004	1.315	2.192	0.634	0.908	0.513
System	4.880	2.589	0.873	1.233	2.312	3.026	5.047	1.458	2.091	1.180
Ground motion	No.11	No.12	No.13	No.14	No.15	No.16	No.17	No.18	No.19	No.20
Bearing	0.518	0.967	2.722	0.884	0.565	1.102	2.114	2.269	0.971	0.365
System	1.192	2.227	6.265	2.036	1.301	2.537	4.867	5.224	2.236	0.841
Ground motion	No.21	No.22	No.23	No.24	No.25	No.26	No.27	No.28	No.29	No.30
Bearing	0.412	1.324	0.805	0.750	1.429	1.146	0.582	0.398	0.203	1.887
System	0.948	3.048	1.853	1.726	3.290	2.638	1.340	0.917	0.468	4.345

CONCLUSION

This paper employs the M-DRM method to compute the fractional moments of the response function in conjunction with the finite element modelling. The method derives the probability distribution of a function of random variables representing the structural response based on the maximum entropy principle. A highway simply-supported bridge was used to validate numerical accuracy and efficiency of the M-DRM method. Then based on OpenSees software, the M-DRM method was used for the structural system reliability assessment of an actual high-pier rigid frame bridge under earthquake loading. Conclusions are drawn in the following:

(1) The linear static and nonlinear dynamic analysis for a simply supported bridge were carried out to validate the numerical accuracy and efficiency of the M-DRM method in comparison with the Monte Carlo simulation. Highly accurate results were obtained via the M-DRM method based on a total of 41 and 46 deterministic model evaluations for both the linear static and nonlinear dynamic analysis, respectively.

(2) The nonlinear FEA model of an actual high-pier railway bridge was used to approximate the probability of failure of structure system using the M-DRM method. The M-DRM method is implemented in OpenSees FEA Software and a total of 1230 deterministic models are evaluated. If the direct Monte Carlo simulation method was used, a total of 10^4 deterministic models should be evaluated at least. The numerical efficiency of M-DRM has been considerably improved by adopting the Gaussian quadrature for the low-dimensional integration.

(3) Uncertainties of structural parameters and ground motions are considered. Under earthquake loading, expansion bearing failure is the primary structural failure mode. For the piers, plastic hinge is formed first at the top section of #1 pier but the serious damage of pier did not occur.

(4) When only component bearing failure is considered, the average bearing failure probability is$1.071*10^{-4}$ under 30 ground motions. When considering a combination of bearing and pier failure, the average structural system failure probability is $2.466*10^{-4}$ under 30 ground motions. Therefore, it is not safe to simply use the failure probability of the component as the failure probability of the structural system.

ACKNOWLEDGMENTS

The research reported in this paper was supported in part by the National Key Basic Research Program of China under Grant No. 2682014CX004EM and the National Natural Science Foundation of China under Grant No.51308465, No.51308473. The authors thank the anonymous reviewers for their constructive comments and advice, which greatly improved the quality of this manuscript.

REFERENCE

Applied Technology Council (ATC). (2008). *ATC-63: Quantification of Building Seismic Performance Factors*. Redwood City, California, US.

Balomenos, G P. & Pandey, M D. (2016). Finite element reliability and sensitivity analysis of structures using the multiplicative dimensional reduction method. *Structure & Infrastructure Engineering*, *12*, 1-13. doi: 10.1080/15732479.2016.1151446

Bartlett, F M., Hong, H P., & Zhou, W. (2003). Load factor calibration for the proposed 2005 edition of the National. *Canadian Journal of Civil Engineering*, *30*, 440-448. doi: 10.1139/L02-08

Bi, K. & Hao, H. (2012). Modelling and simulation of spatially varying earthquake ground motions at sites with varying conditions. *Probabilistic Engineering Mechanics*, *29*, 92-104. doi: 10.1016/j.probengmech.2011.09.002

591 Cimellaro, G., Reinhorn, A., Bruneau, M., & Rutenberg, A. (2006). *Multidimensional fragility of structures:*
592 *formulation and evaluation* (Report No. MCEER-06-0002), New York: University at Buffalo - the State
593 University of New York.
594 Caglayan, O., Ozakgul, K., Tezer, O., & Uzgider, E. (2011). Evaluation of a steel railway bridge for dynamic
595 and seismic loads. *Journal of Constructional Steel Research, 67,* 1198-1211. doi: 10.1016/j.jcsr.2011.02.013
596 CCCC Highway Consultants CO., Ltd (HPDI). (2004). *General Code for Design of Highway Bridges and*
597 *Culverts (JTG D60-2004)*, Beijing: People communication press. (In Chinese)
598 Cheng, C. T., Yang, J. C., Yeh, Y. K., & Chen, S. E. (2003). Seismic performance of repaired hollow-bridge
599 piers. *Construction & Building Materials, 17,* 339–351. doi: 10.1016/S0950-0618(02)00119-8
600 Ditlevsen, O. & Madsen, H.O. (1996). *Structural reliability methods*. New York: John Wiley & Sons
601 Publication.
602 Ellingwood, B R. & Rajashekhar, M R. (1995). Reliability of Reinforced-Concrete Cylindrical Shells. *Journal*
603 *of Structural Engineering, 121,* 336-347. doi: 10.1061/ (ASCE) 0733-9445(1995)121:2(336)
604 Faravelli, L. (1989). A response surface approach for reliability analysis. *Journal of Engineering Mechanics,*
605 *115*, 2763-2781. doi: 10.1061/ (ASCE) 0733-9399(1989)115:12(2763)
606 Frangopol, Dan M. (2008). Probability concepts in engineering: emphasis on applications to civil and
607 environmental engineering. *Structure & Infrastructure Engineering, 4*, 413-414. doi:
608 10.1080/15732470802027894
609 Guizhou Seismological Bureau (GSB). (2010). *Seismic Safety Assessment Report for Chahe Railway Bridge*
610 [S]. Guiyang, Guizhou Province, China. (In Chinese)
611 Hwang, H., Liu, J. B., & Chiu, Y. H. (2001). *Seismic Fragility Analysis of Highway Bridges*. Memphis: Center
612 for Earthquake Research and Information, the University of Memphis.
613 Jaynes, E T. (1957). Information Theory and Statistical Mechanics. *Physical Review, 106,* 620-630. doi:
614 10.1103/PhysRev.106.620
615 Li, J., Chen, J., & Fan, W., (2007). The equivalent extreme-value event and evaluation of the structural system
616 reliability. *Structural Safety, 29,* 112-131. Doi:10.1016/j.strusafe.2006.03.002.

Liang, Z. (2007). *Study on seismic design theory of irregular girder bridge with high piers*. Tongji University, Shanghai. (In Chinese)

Madsen, H O., Krenk S., & Lind N C. (2006). *Methods of Structural Safety*. New York: Dover Publications.

Mazzoni, S., McKenna, F., Scott, M.H. & Fenves, G.L., (2006). *OpenSees command language manual.* Berkeley: Pacific Earthquake Engineering Research Centre.

Matthew, D. & Greg, F. (2008). *Numerical simulation of Bridge model*. Berkeley: University of California, Berkeley.

Mirza, S. A., & Skrabek, B. W. (1991). Reliability of short composite beam-column strength interaction. *Journal of Structural Engineering, 117*, 2320-2339. doi: 10.1061/ (ASCE) 0733-9445(1991)117:8(2320)

Ministry of Railways of China (MRC). (2005). *Fundamental code for design on railway bridge and culvert (J460-2005)*, Beijing: Chinese railway press. (In Chinese)

Ministry of Railways of China (MRC). (2006). *Code for seismic design of railway engineering: GB 50111-2006*. Beijing: Chinese Planning Press. (In Chinese)

Ministry of Transport of China (MTC). (2008).*Guidelines for Seismic Design of Highway Bridges (JTG/T B02-01-2008)*, Beijing: People communication press. (In Chinese)

Ministry of Railways of China (MRC). (2013). *Pot bearings for railway bridges (TB/T 2331-2013)*, Beijing: Chinese railway press. (In Chinese)

Nielson, B. G. & Desroches, R. (2007). Analytical seismic fragility curves for typical bridges in the central and south eastern United States. *Earthquake Spectra, 23*, 615-633.Doi: 10.1193/1.2756815

Nowak, A. S., Nowak, S., & Szerszen, M. M. (2003). Calibration of design code for buildings (ACI 318): part 1 - statistical models for resistance. *American Concrete Institute Structural Journal, 100*, 377-382.

Nowak, A. S., Rakoczy, A. M., & Szeliga, E. K. (2011). Revised statistical resistance models for R/C structural components. Michigan: American Concrete Institute Special Publication.

Rackwitz, R. (2001). Reliability analysis -a review and some perspectives. *Structural Safety, 23*, 365-395. doi: 10.1016/S0167-4730(02)00009-7

642 Rahman, S. & Xu, H. (2004). A univariate dimension-reduction method for multi-dimensional integration in
643 stochastic mechanics. *International Journal for Numerical Methods in Engineering*, *61*, 1992-2019. doi:
644 10.1016/j.probengmech.2004.04.003
645 Rubinstein, R Y. (2008). *Simulation and the Monte Carlo Method*. New York: John Wiley & Sons Publication.
646 Sudret, B. & Kiureghian, A D. (2002). Comparison of finite element reliability methods. *Probabilistic*
647 *Engineering Mechanics*, *17*, 337-348. Doi: 10.1016/S0266-8920(02)00031-0
648 Wang, Z. (2008). A preliminary report on the Great Wenchuan Earthquake. *Earthquake Engineering and*
649 *Engineering Vibration*, *7*, 225-234. (In Chinese)
650 Wei, D. & Rahman, S. (2010). A multi-point univariate decomposition method for structural reliability analysis.
651 *International Journal of Pressure Vessels & Piping*, *87*, 220-229. doi: 10.1016/j.ijpvp.2010.03.021
652 Zhang, X. & Pandey, M D. (2013). Structural reliability analysis based on the concepts of entropy, fractional
653 moment and dimensional reduction method. *Structural Safety*, *43*, 28–40. doi: 10.1016/j.strusafe.2013.03.001
654 Zhang, X., Pandey, M D., & Zhang, Y. (2011). A numerical method for structural uncertainty response
655 computation. *Science China Technological Sciences*, *54*, 3347-3357. doi: 10.1007/s11431-011-4603-x
656 Zhao, W., Liu, W., & Yang, Q. (2016). An improvement of the response surface method based on reference
657 points for structural reliability analysis. *KSCE Journal of Civil Engineering*, *20*, 1-8. doi: 10.1007/s12205-
658 016-1312-9
659 Zheng, Y. & Das, P K. (2000). Improved response surface method and its application to stiffened plate
660 reliability analysis. *Engineering Structures*, *22*, 544–551. doi: 10.1016/S0141-0296(98)00136-9
661